



OPEN

Enhanced photocatalytic performance of TiO₂-ZnO hybrid nanostructures

SUBJECT AREAS:
STRUCTURAL PROPERTIES
NANOWIRESChun Cheng^{1*}, Abbas Amini^{2*}, Chao Zhu³, Zuli Xu³, Haisheng Song⁴ & Ning Wang³Received
5 November 2013Accepted
7 February 2014Published
25 February 2014Correspondence and
requests for materials
should be addressed to
C.C. (cheng.c@sustc.
edu.cn) or N.W.
(phwang@ust.hk)* These authors
contributed equally to
this work.

¹Department of Materials Science and Engineering, South University of Science and Technology, Shenzhen, 518055, China, ²Institute for Frontier Materials, Deakin University, Waurn Ponds, VIC 3217, Australia, ³Department of Physics, Hong Kong University of Science and Technology, Hong Kong, China, ⁴Wuhan National Laboratory for Optoelectronics (WNLO) and the School of Optical and Electronic Information, Huazhong University of Science and Technology, Wuhan 430074, China.

We studied the photocatalytic properties of rational designed TiO₂-ZnO hybrid nanostructures, which were fabricated by the site-specific deposition of amorphous TiO₂ on the tips of ZnO nanorods. Compared with the pure components of ZnO nanorods and amorphous TiO₂ nanoparticles, these TiO₂-ZnO hybrid nanostructures demonstrated a higher catalytic activity. The strong green emission quenching observed from photoluminescence of TiO₂-ZnO hybrid nanostructures implied an enhanced charge transfer/separation process resulting from the novel type II heterostructures with fine interfaces. The catalytic performance of annealing products with different TiO₂ phase varied with the annealing temperatures. This is attributed to the combinational changes in E_g of the TiO₂ phase, the specific surface area and the quantity of surface hydroxyl groups.

Semiconductor nanostructured composites draw intensive interests because of their improved properties and promising technological applications, such as photochemical solar cells, photo catalysts, photosensors, electro-luminescent displays, and biolabels. In recent years, considerable effort has been exerted toward combining semiconductor nanostructures with suitable materials to synergize their properties. For example, the deposition of metals or metallic islands on ZnO and TiO₂ nanostructures can result in an enhanced photocatalytic performance¹⁻⁴. Generally, photocatalytic efficiency is limited by a fast recombination of photogenerated charge carriers. In semiconductor/metal nanocomposites, the metal component can trap the photo-induced charge carriers and consequently promotes the interfacial charge-transfer processes¹. Compared to the single element of ZnO and TiO₂, coupled ZnO/TiO₂ composite displays a largely improved photocatalytic activity, such as in the degradation of phenol, 2-chlorophenol, and pentachlorophenol⁵ and in the decomposition of salicylic acid⁶. This enhanced photocatalytic behavior is attributed to the efficient spatial separation of electrons and holes⁷. However, previous research works mainly studied the coupled ZnO/TiO₂ with a simple core-shell structure (coated surface) or sandwich geometry (randomly adhered particles). Inappropriate structures of the interface in these two structures limit the interfacial charge-transfer process of photogenerated charge carriers and thus lower the photocatalytic property of the nanocomposite materials⁸⁻¹¹. As such, challenges still remain in fabricating these nanohybrids with desirable interfacial structures. We have recently developed a simple method to build TiO₂-ZnO (TZO) nanohybrid structures by a site-specific deposition of titanium oxide on ZnO nanorods (NRs)¹². The TZO nanohybrids show uniform and atomically flat interfaces between ZnO and TiO₂ with tunable crystal phases, which are amorphous, anatase and rutile. These TZO nanohybrid structures are expected to demonstrate an enhanced photocatalytic behavior. This is due to the improved interfacial structures which suit better the charge-transfer and spatial separation processes of photogenerated charge carriers. In this paper, we study the photocatalytic behaviors of TZO products and their annealed products with different TiO₂ phase structures. The aim is to elucidate the relationship between various TZO structures and their photocatalytic properties.

Results

Figure 1 shows the XRD patterns of the produced TZO and the annealed TZOs, TZO300 and TZO600. The presence of Wurtzite-type hexagonal-phase ZnO is clearly shown in all samples with the lattice parameters $a = 3.252 \text{ \AA}$ and $c = 5.208 \text{ \AA}$. These data are in good agreement with the calculated values $a = 3.253$ and $c = 5.209$ (JCPDS 80-0075). There are no apparent peaks for anatase and rutile TiO₂ in the XRD patterns of the annealed products. As the quantity of TiO₂ coupled with ZnO NRs is very small, less than ~5 wt%, the XRD cannot detect them in the annealed substances.

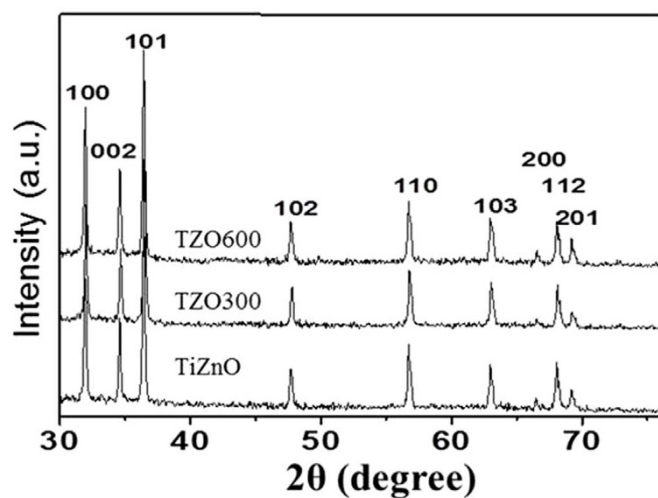


Figure 1 | XRD patterns of TZO, TZO300 and TZO600. The prominent sharp peaks in all products are attributed to Wurtzite ZnO.

The scanning electron microscopy images of TZO products in Fig. 2a reveal that TiO₂ NPs with diameters in the range of 20–250 nm are deposited on one of the frontier ends of ZnO NRs. These ZnO NRs have diameters in the range of 10–200 nm and lengths in the range of 1–3 μm. Fig. 2 shows that the typical

morphology of a single TZO nano hybrid containing a cap-like TiO₂ NP which covers one end of the ZnO NR. The ZnO NRs are well crystallized with no detected impurities in the EDX results. The titanium oxide particles assembled with NRs are identified as amorphous, and the stoichiometric ratio of Ti to O is approximately 1 : 2 as measured by EDS (see Fig. 2b). The interfaces between ZnO NRs and TiO₂ are flat and clearly visible when the electron beam is perpendicular to the NRs axes. After annealing, the products are still well dispersed and the morphologies do not change (Fig. 2c and d) while the amorphous TiO₂ caps have transformed to the anatase and rutile phases. The interface structures of almost all of the nano hybrids are similar and atomically flat. Readers can refer to our previous work^{12,13} for more details about the formation mechanism of TZO and related structural characterizations.

The UV-Vis absorption spectra of amorphous TiO₂ NPs, ZnO NRs, TZO nano hybrids and the annealed products at 300 °C (TZO300) and 600 °C (TZO600) are compared in Fig. 3. ZnO NRs and all TZOs have strong adsorption in the UV region at the absorption edge of ca. 380 nm, with a corresponding ZnO bandgap of 3.26 eV. The amorphous TiO₂ NPs have a strong adsorption in the deep-UV region at the absorption edge ca. 313 nm with a corresponding bandgap of 3.96 eV^{14,15}. For TZO, a higher absorbance below 320 nm ensures that the TiO₂ NPs, which are attached to ZnO NRs, dominate the deep UV absorption. This may enhance the use of UV light compared with pure ZnO NRs.

Other studies on semiconductor-semiconductor and semiconductor-metal composites such as CdS-ZnO¹⁶, CdS-SWCNT¹⁷,

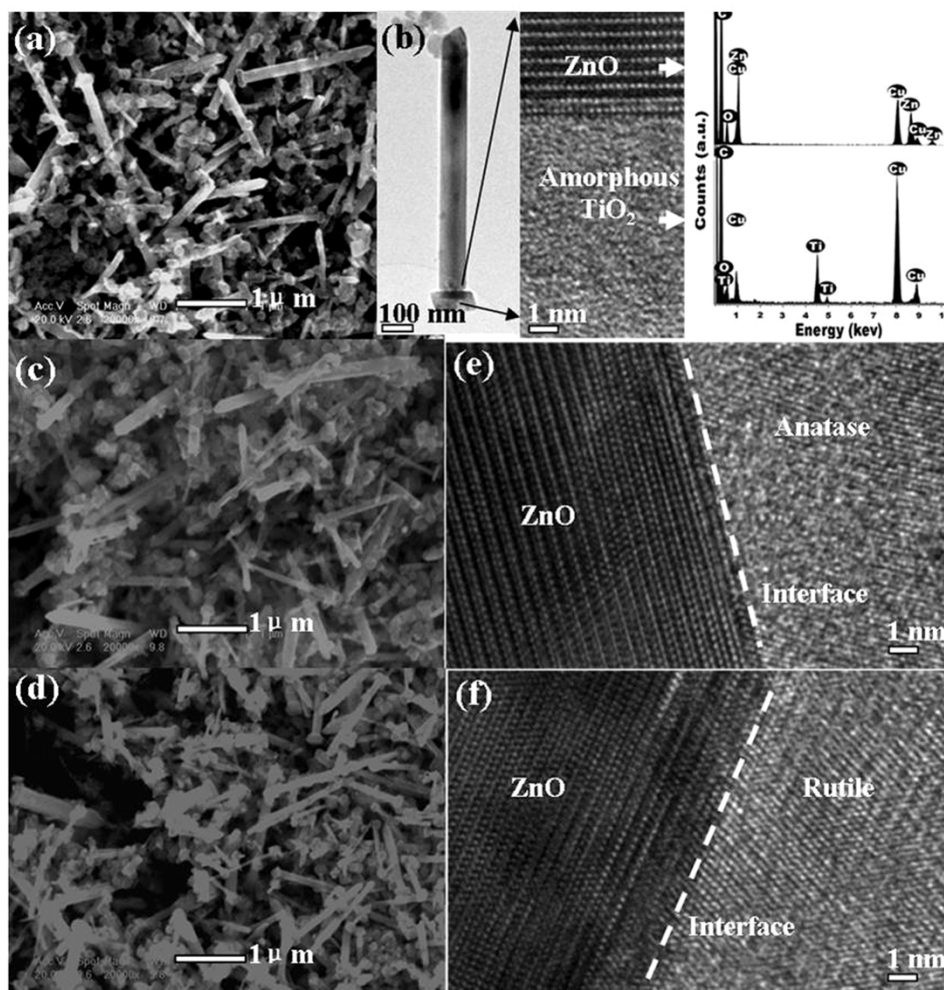


Figure 2 | (a) SEM image of TZO, (b) TEM and HRTEM images of a TZO and its EDS spectra, (c) and (d) SEM images of TZO300 and TZO600, (e) and (f) HRTEM images of TZO300 and TZO600, displaying the fine structures of the interface.

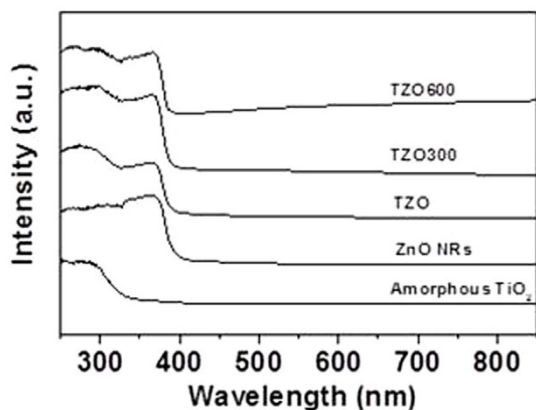


Figure 3 | UV-Vis absorption spectra of amorphous TiO₂ NPs, ZnO NRs, TZO nano hybrids and the annealed products TZO300 and TZO600.

ZnO-SWCNT¹⁸, CdS-AgI¹⁹, CdS-TiO₂²⁰, TiO₂-Au^{21,22}, and ZnO-Au^{23,24} have shown a charge equilibration when they are subjected to a bandgap excitation. Photo-induced electron transfer between composites can be initiated by the examined emission quenching (as shown in references 16–24). ZnO NRs with a bandgap of 3.26 eV undergo charge separation under UV-excitation ($\lambda < 380$ nm). These charge carriers (e_{CB} and h_{VB}) can be either directly recombined or trapped in the vacancies (e_i and h_t)¹⁸. Research has shown that the green emission from ZnO colloids originates from oxygen vacancies²⁵. The green emission with a maximum of ~ 525 nm is a useful probe to monitor the charge transfer process on the ZnO surface. In the present study we monitor the green emission from ZnO to investigate the charge transfer interaction with TiO₂. Fig. 4 shows the PL spectra of ZnO NRs and TZO nano hybrids. Due to the site-specific assembly of TiO₂ NPs on ZnO NRs with fine interfaces, ZnO NRs are expected to intensely interact with the deposited TiO₂, and as a result of this interaction we expect a decrease in the emission yield of ZnO. Indeed, due to this interaction, a significant decrease, \sim ca. 50%, in the emission yield of the TZO nano hybrids is observed compared with that of pure ZnO NRs as shown in Fig. 4.

Now, to evaluate the photo-oxidation capability of TZO nano hybrids, we examine the decomposition of MB dye in solution over the samples TZO, TZO300, and TZO600 under UV light irradiation as a function of time (Fig. 5). For comparison, we carried out the decomposition of the MB dye in a solution over two reference photocatalysts, amorphous TiO₂ NPs and ZnO NRs under UV light irradiation

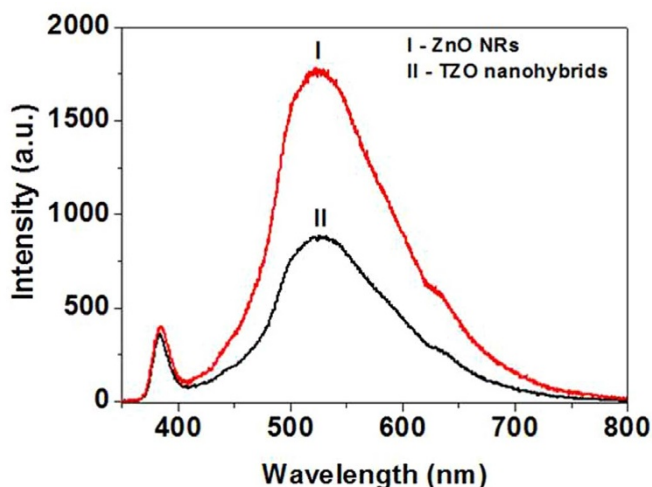


Figure 4 | PL spectra of (I) ZnO NRs and (II) TZO nano hybrids.

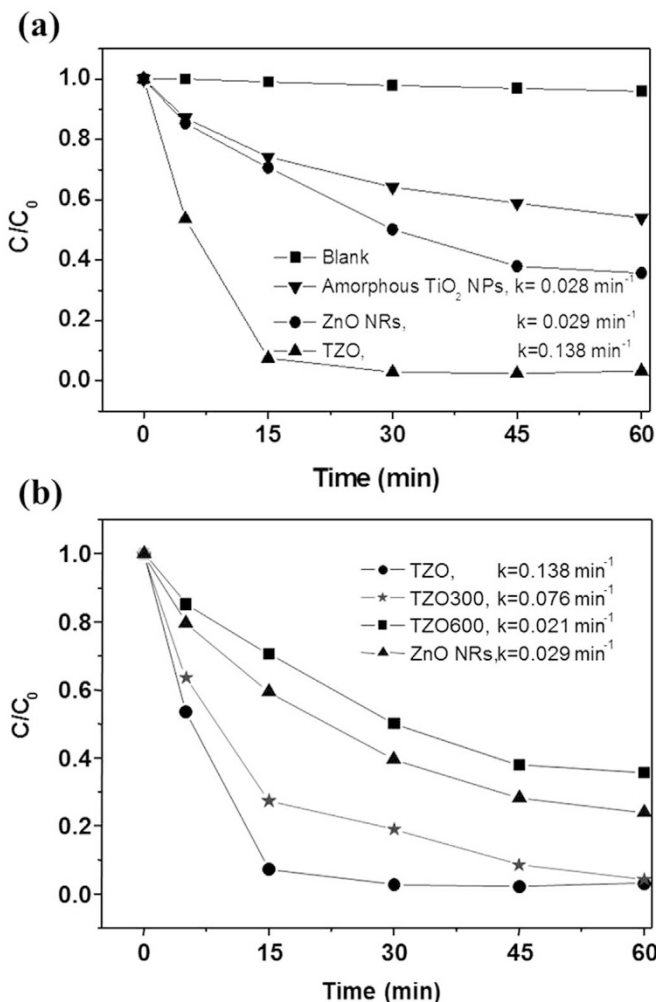


Figure 5 | (a) Photodegradation of MB by amorphous TZO products, ZnO NRs, amorphous TiO₂ NPs and blank experiment. (b) A comparison of the photocatalytic properties of ZnO NRs, TZO, TZO300 and TZO600.

(Fig. 5a). To show that the decomposition of MB dye over TZO is caused neither by catalysis nor photolysis, we carried out a decomposition experiment in a dark environment with TZO as well as under a full arc light irradiation (with no catalyst, blank experiment in Fig. 5a). In these experiments, the MB concentration remained unchanged as a function of time, that is, TZO is an active catalyst under UV light. From an exponential decay at the initial stage (0–15 min), the decomposition kinetics follows a first order kinetics with the classical equation $\ln(C/C_0) = -k \cdot t$, where k is the so-called pseudo-first rate kinetic constant, C_0 is the initial concentration and C is the concentration after the MB degradation for time t . The presented k values in Fig. 5 are from fitting curves of the data for a 0–15 min period. These values represent a good measurement of the overall photo-degradation rate of all the investigated structures. TZO, with $k = 0.138 \text{ min}^{-1}$ which is about five times that of ZnO NRs, has the fastest MB decomposition rate. The photocatalytic activities of annealed products TZO300 and TZO600 decrease when the annealing temperature increases with the TiO₂ phase on the TZO nano hybrid structures transformed from the amorphous to anatase and rutile phases.

Discussion

The TZO nano hybrids form a type II semiconductor heterostructure²⁶ as shown in Fig. 6. In this case, electrons and holes in semiconductors are at their lowest energy states. Therefore, the energy gradient at the

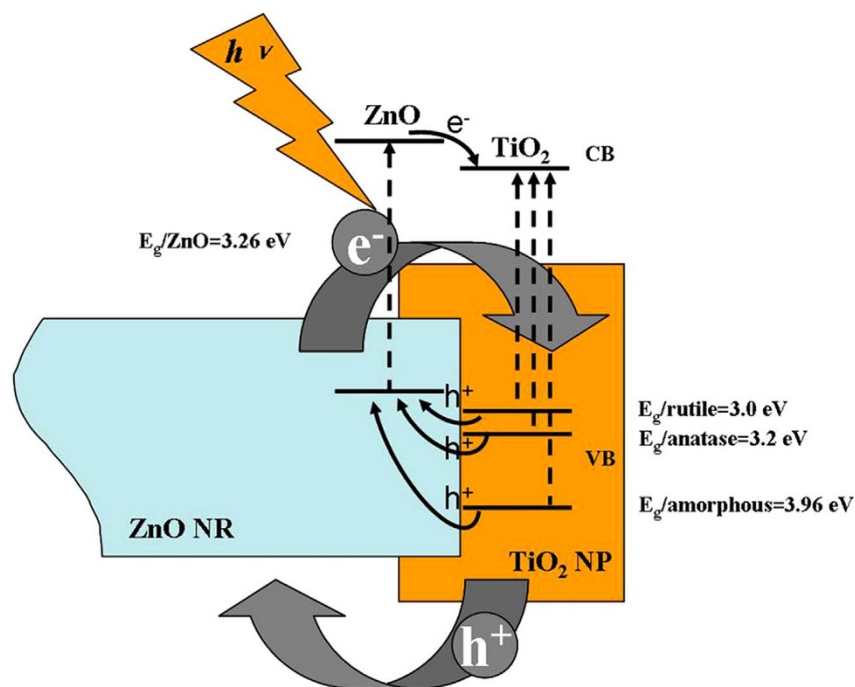


Figure 6 | Illustration of photo-induced charge transfer and separation at the interface of TZO heterostructures.

interfaces tends to spatially separate those electrons and holes which are excited by UV light on different sides of the hetero-junction. Under illumination, the electrons are transferred from the conduction band (CB) of ZnO to CB of TiO₂. In addition, the holes are transferred from the valence band (VB) of TiO₂ to VB of ZnO. This process isolates active electrons and holes and, hence, accelerates the decrease in the electron-hole pair recombination and erodes the increase in lifespan. These phenomena directly result in an intense emission quenching as revealed by the PL results in Fig. 4. They also increase the availability of the pairs (electron and hole) on the surface of the photocatalysts and thus enhance the redox process. Significantly, the fine atomic flat interfaces across TiO₂ and ZnO of TZO nano hybrids ease this charge transfer/isolation process by a decreased interface resistance. In addition, the elongated one dimensional structure of ZnO nanorods also helps to decrease the recombination probability of photogenerated carriers due to an increased delocalization of electrons²⁷. Therefore, our special TZO structures favor the photocatalytic process not only by the band structure configurations but also by the fine interface structures and geometrical structures between the two components TiO₂ and ZnO.

It is worthwhile to explain the rationale for the degeneration of the TZOs photocatalytic property sourced from the annealing treatment. First, as shown in Fig. 6, a larger energy gradient between VB_{ZnO} and VB_{TiO₂} is apparently more beneficial for the transfer of active holes from TiO₂ to ZnO. This difference is reduced as the bandgap energy (E_g) of TiO₂ structures drops after annealing treatments ($E_{g/\text{rutile}} (3.0 \text{ eV}) < E_{g/\text{anatase}} (3.2 \text{ eV}) < E_{g/\text{amorphous}} (3.96 \text{ eV})$). Hence, the ability of the charge transfer/separation is consequently weakened. Second, specific surface area and surface hydroxyl groups can strongly affect photocatalytic activities of nanomaterials and, sometimes, they are the dominating factors compared with the crystal structure²⁸. In the present case, an increase in annealing temperature results in a decrease in the specific surface area of TZOs (TZO 14.643 m²/g; TZO300 13.763 m²/g; TZO600 8.418 m²/g). This temperature variation also decreases the quantity of the surface of hydroxyl groups (See caption of Fig. 7) which slows the photocatalytic activities. Nevertheless, the reaction rates of annealed TZOs are relatively higher than or close to that for ZnO NRs. These rationales determine the enhanced photocatalytic activities of TZOs.

In conclusion, this paper investigates the photocatalytic properties of TZOs and their annealed products with different TiO₂ phases. Compared with the components of ZnO NRs and amorphous TiO₂ NPs, the combined TZOs demonstrated higher catalytic activities. This is explained by an enhanced charge transfer/separation process resulting from the novel type II heterostructures with fine interfaces, and supported by the emission quenching mechanism in the PL studies. The catalytic performance of annealing products varied with the annealing temperatures. This originated from the combinational changes in E_g of the TiO₂ phase, the specific surface area and the quantity of surface hydroxyl groups. Our investigation suggests an effective type of hybrid nanostructures for photocatalytic applications and other applications such as photodetectors and solar cells.

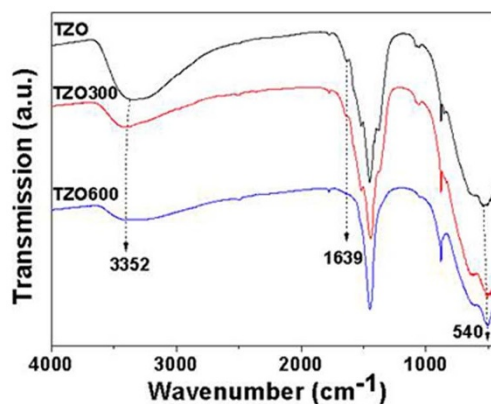


Figure 7 | FTIR spectra of as-synthesized TZO, TZO300 and TZO600 samples in the wavenumber range of 4000–400 cm⁻¹. The broad absorptions at about 3352 and 1639 cm⁻¹ are assigned to the hydroxyl groups of chemisorbed and/or physisorbed H₂O molecules on the samples. A strong absorption band near 540 cm⁻¹ reveals the vibration properties of ZnO NRs. Other unsigned peaks are attributed to remnant organic species in the samples.



Methods

The method for the fabrication of TZO nanohybrid structures is similar to that described in our recent work¹² and consists of three steps: 1) Preparation of ZnO NRs: 5 mL of 0.1 M zinc acetate ethanol solution was mixed with 35 mL of 0.5 M NaOH ethanol solution to form a suspension solution. The suspension solution was later transferred to a 50 mL Teflon-lined stainless steel autoclave and kept at 180 °C for 24 hours. 2) Preparation of sodium titanate nanotubes: 1 g of anatase TiO₂ NPs were treated with a NaOH (10 M) aqueous solution in a Teflon vessel at 150 °C for 12 hours²⁹. 3) 200 mg sodium titanate nanotubes are mixed with the final reacted solution from step 1 and kept at 180 °C for another 24 hours. Off-white precipitation products, obtained at the bottom of the autoclave, were sonicated for 30 minutes and then allowed to stand for another 30 minutes in order to separate them into two layers. The upper white TZO and the lower off-white superfluous amorphous TiO₂ NPs were collected separately and washed with ethanol and DI water, centrifuged and dried at 80 °C. The annealed TZO were also prepared by heating the as-prepared TZO at 300 °C (TZO300) and 600 °C (TZO600) for 2 hours in air to convert the amorphous TiO₂ NPs to the anatase and rutile phase, respectively. The crystallization of as-prepared samples was characterized by X-ray diffraction (XRD, Philips, PW1813). Morphology and structure characterizations were carried out using a scanning electron microscope (SEM, Philips XL-30) and a high-resolution transmission electron microscope (HRTEM, JEOL 2010F) equipped with an energy-dispersive X-ray spectrometer (EDS). The photoluminescence (PL) was measured by a 325 nm He-Cd laser as the exciting light source. UV-Vis absorption spectrum measurement was conducted using a UV-Vis spectrophotometer (Lambda 20) and an integrating sphere (Labsphere) with a sampling spot of 10 mm × 10 mm at normal incidence. The surface area was characterized using a Brunauer-Emmett-Teller (BET) machine and a surface-pore size analyzer (Beckman Coulter, SA 3100). Chemical bonding information of the samples was obtained using a Fourier transform infrared spectrometer (FTIR; Bio-Rad, FTS 600). For the photocatalytic measurement, 80 mg of each catalyst was suspended in 200 mL of a methylene blue (MB) aqueous solution (20 ppm). The mixture was poured into a quartz tube and kept in a dark environment for 30 minutes to allow it to attain an equilibrium adsorption state. The concentration of the MB solution slightly decreased while it was in the dark room with the C₀ value slightly lower than 20 ppm at t = 0. UV irradiation was carried out using a 500 W high-pressure Hg lamp (with the strongest emission at 368 nm) and cooling by cycling water. After a set irradiation time, ~3 mL of the mixture was withdrawn, and the catalysts were separated from the suspensions by a centrifuge. The degradation process was monitored by the UV-Vis spectrophotometer measuring the absorption of MB at 664 nm.

- Sheng, F. *et al.* Simulation on field enhanced electron transfer between the interface of ZnO–Ag nanocomposite. *J. Phys. Chem. C* **117**, 18627–18633 (2013).
- Gu, C. D. *et al.* Growth and photocatalytic activity of dendrite-like ZnO@Ag heterostructure nanocrystals *Cryst. Growth Des.* **9**, 3278–3285 (2009).
- Han, Y. *et al.* TiO₂ supported Pd@Ag as highly selective catalysts for hydrogenation of acetylene in excess ethylene *Chem. Commun.* **49**, 8350–8352 (2013).
- Zheng, Y. H. *et al.* Ag/ZnO heterostructure nanocrystals: synthesis, characterization, and photocatalysis. *Inorg. Chem.* **46**, 6980–6986 (2007).
- Serpone, N., Maruthamuthu, P., Pichat, P., Pelizzetti, E. & Hidaka, H. Exploiting the interparticle electron transfer process in the photocatalysed oxidation of phenol, 2-chlorophenol and pentachlorophenol: chemical evidence for electron and hole transfer between coupled semiconductors. *J. Photochem. Photobiol. A: Chem.* **85**, 247–255 (1995).
- Sukharev, V. & Kershaw, R. Concerning the role of oxygen in photocatalytic decomposition of salicylic acid in water. *J. Photochem. Photobiol. A: Chem.* **98**, 165–169 (1996).
- Marci, G. *et al.* Preparation characterization and photocatalytic activity of polycrystalline ZnO/TiO₂ systems. 2 surface, bulk characterization, and 4-nitrophenol photodegradation in liquid-solid regime. *J. Phys. Chem. B* **105**, 1033–1040 (2001).
- Chueh, Y. L., Chou, L. J. & Wang, Z. L. SiO₂/Ta₂O₅ core-shell nanowires and nanotubes. *Angew. Chem. Int. Ed.* **45**, 7773–7778 (2006).
- Shi, W. *et al.* A general approach to binary and ternary hybrid nanocrystals. *Nano Lett.* **6**, 875–881 (2006).
- Kwon, K.-W. & Shim, M. Gamma-Fe₂O₃/II-VI sulfide nanocrystal heterojunctions. *J. Am. Chem. Soc.* **127**, 10269–10275 (2005).
- Casavola, M. *et al.* Topologically controlled growth of magnetic-metal-functionalized semiconductor oxide nanorods. *Nano Lett.* **7**, 1386–1395 (2007).
- Cheng, C., Yu, K. F., Cai, Y., Fung, K. K. & Wang, N. Site-specific deposition of titanium oxide on zinc oxide nanorods. *J. Phys. Chem. C* **111**, 16712–16716 (2007).

- Cheng, C. *et al.* Zn₂TiO₄–ZnO Nanowire Axial Heterostructures Formed by Unilateral Diffusion. *J. Phys. Chem. C* **115**, 78–82 (2010).
- Naik, V. M., Haddad, D., Naik, R., Benci, J. & Auner, G. W. Optical properties of anatase, rutile and amorphous phases of TiO₂ thin films grown at room temperature by RF magnetron sputtering. *Mat. Res. Soc. Symp. Proc.* **755**, DD11.12.1–6 (2003).
- David, M. K., Du, X., Cavanagh, A. S. & Weimer, A. W. Quantum confinement in amorphous TiO₂ films studied via atomic layer deposition. *Nanotechnology* **19**, 445401 (2008).
- Hotchandani, S. & Kamat, P. V. Charge-transfer processes in coupled semiconductor systems. Photochemistry and photoelectrochemistry of the colloidal cadmium sulfide-zinc oxide system. *J. Phys. Chem.* **96**, 6834–6839 (1992).
- Robel, I., Bunker, B. & Kamat, P. V. Single-walled carbon nanotube-CdS nanocomposites as light-harvesting assemblies: Photoinduced charge-transfer interactions. *Adv. Mater.* **17**, 2458–2463 (2005).
- Vietmeyer, F., Seger, B. & Kamat, P. V. Excited state interactions and charge collection. *Adv. Mater.* **19**, 2935–2940 (2007).
- Gopidas, K. R., Bohorquez, M. & Kamat, P. V. Charge-transfer processes in colloidal CdS-TiO₂ and CdS-AgI systems. *J. Phys. Chem.* **94**, 6435–6440 (1990).
- Sant, P. A. & Kamat, P. V. Interparticle electron transfer between size-quantized CdS and TiO₂ semiconductor nanoclusters. *Phys. Chem. Chem. Phys.* **4**, 198–203 (2002).
- Jakob, M., Levanon, H. & Kamat, P. V. Charge distribution between UV-Irradiated TiO₂ and gold nanoparticles: determination of shift in the Fermi level. *Nano Lett.* **3**, 353–358 (2003).
- Subramanian, V., Wolf, E. E. & Kamat, P. V. Catalysis with TiO₂/gold nanocomposites. *J. Am. Chem. Soc.* **126**, 4943–4950 (2004).
- Wood, A., Giersig, M. & Mulvaney, P. Fermi level equilibration in quantum dot-metal nanojunctions. *J. Phys. Chem. B* **105**, 8810–8815 (2001).
- Subramanian, V., Wolf, E. E. & Kamat, P. V. Green emission to probe photoinduced charging events in ZnO–Au nanoparticles. Charge distribution and fermi-level equilibration. *J. Phys. Chem. B* **107**, 7479–7485 (2003).
- Djurisic, A. B. & Leung, Y. H. Optical properties of ZnO nanostructures. *Small* **2**, 944–961 (2006).
- Ivanov, S. A. *et al.* Type-II core/shell CdS/ZnSe nanocrystals: synthesis, electronic structures, and spectroscopic properties. *J. Am. Chem. Soc.* **129**, 11708–11719 (2007).
- Leelavathi, A., Madrasa, G. & Ravishankar, N. Origin of enhanced photocatalytic activity and photoconduction in high aspect ratio ZnO nanorods. *Phys. Chem. Chem. Phys.* **15**, 10795–802 (2013).
- Li, Y., Sasaki, T., Shimizu, Y. & Koshizaki, N. Hexagonal-close-packed, hierarchical amorphous TiO₂ nanocolumn arrays: transferability, enhanced photocatalytic activity, and superamphiphilicity without UV irradiation. *J. Am. Chem. Soc.* **130**, 14755–14762 (2008).
- Yao, B. D. *et al.* Formation mechanism of sodium titanate nanotubes. *Appl. Phys. Lett.* **82**, 281–283 (2003).

Acknowledgments

Financial support from the Hong Kong Research Grants Council through RGC projects (No. FSGRF12SC22 and WMINST11SC04) and starting grants from South University of Science and Technology of China are gratefully acknowledged.

Author contributions

C.C. designed the research, performed TEM characterizations, and photocatalytic experiments, analysed the results and wrote the paper. A.A. and Z.X. performed the XRD and UV-Vis spectrophotometer characterization and the paper revision. C.Z. performed the nonmaterial fabrication. H.S. incorporated in the interpretation of experimental results. N.W. contributed significant discussion and final paper polishing.

Additional information

Competing financial interests: The authors declare no competing financial interests.

How to cite this article: Cheng, C. *et al.* Enhanced photocatalytic performance of TiO₂–ZnO hybrid nanostructures. *Sci. Rep.* **4**, 4181; DOI:10.1038/srep04181 (2014).



This work is licensed under a Creative Commons Attribution 3.0 Unported license. To view a copy of this license, visit <http://creativecommons.org/licenses/by/3.0>